Magnetic phase diagram of the frustrated $S = 1/2$ chain magnet $LiCu_2O_2$

A.A. Bush,[1] V.N. Glazkov,[2,3] M. Hagiwara,[4] T. Kashiwagi,[5] S. Kimura,[6]
K. Omura,[4] L.A. Prozorova,[2] L.E. Svistov,[2,4,*] A.M. Vasiliev,[2] and A. Zheludev[3]

[1]*Moscow Institute of Radioengineering, Electronics and Automation, 117454 Moscow, Russia*
[2]*P. L. Kapitza Institute for Physical Problems RAS, 119334 Moscow, Russia*
[3]*Neutron Scattering and Magnetism, Laboratory for Solid State Physics, ETH Zurich, Switzerland, 8093 Zürich, Switzerland*
[4]*KYOKUGEN, Osaka University, Machikaneyama 1-3, Toyanaka 560-8531, Japan*
[5]*Institute for Materials Science and Graduate School of Pure and Applied Sciences, University of Tsukuba, 1-1-1 Tennodai, Tsukuba, Ibaraki 305-8573, Japan*
[6]*Institute for Materials Research, Tohoku University, 2-1-1 Katahira, Sendai, Miyagi 980-8577, Japan*

(Dated: March 15, 2012)

We present the results of the magnetization and dielectric constant measurements on untwinned single crystal samples of the frustrated $S = 1/2$ chain cuprate $LiCu_2O_2$. Novel magnetic phase transitions were observed. A spin flop transition of the spiral spin plane was observed for the field orientations $\boldsymbol{H} \parallel \boldsymbol{a}$, $\boldsymbol{b}$. The second magnetic transition was observed at $H \approx 15$ T for all three principal field directions. This high field magnetic phase is discussed as a collinear spin-modulated phase which is expected for an S=1/2 nearest-neighbor ferromagnetic and next-nearest-neighbor antiferromagnetic chain system.

PACS numbers: 75.50.Ee, 76.60.-k, 75.10.Jm, 75.10.Pq

I. INTRODUCTION

Unconventional magnetic orders and phases in frustrated quantum–spin chains are one of the attractive issues, because they appear under a fine balance of the exchange interactions and are sometimes caused by much weaker interactions or fluctuations[1–5].

A kind of frustration in quasi–one–dimensional (1D) chain magnets is provided by competing interactions when the nearest neighbor (NN) exchange is ferromagnetic and the next–nearest neighbor (NNN) exchange is antiferromagnetic. Numerical investigations of the frustrated chain magnets within different models[6–9] have predicted a number of exotic magnetic phases in the magnetization process such as planar spiral and different multipolar phases. Theoretical studies of the magnetic phase diagram show that the magnetic phases are very sensitive to the interchain interactions and anisotropic interactions in the system[10–14].

There are a number of magnets which are attractive objects for the experimental investigations as realizations of one-dimensional frustrated systems: $LiCuVO_4$, $Rb_2Cu_2Mo_3O_{12}$, Li_2ZrCuO_4, $CuCl_2$, Li_2CuO_2, $LiCu_2O_2$, $NaCu_2O_2$ (see for example, Refs.15–19). Some of these magnets, such as $LiCuVO_4$, Li_2CuO_2 and Li_2ZrCuO_4, are quasi–one–dimensional magnets, while others are quasi–two–dimensional magnets with the layers of frustrated chains.

In the present paper, we report the results of magnetization and dielectric constant measurements on the quasi two dimensional antiferromagnet $LiCu_2O_2$. Our new experiments expand the magnetic field range from the fields of up to 9 T of the previous work[20] to the fields of up to 52 T, which is approximately 40% of the expected saturation field (H_{sat}). These measurements display two phase transitions. The low field transition may be interpreted as a spin-flop transition while the novel high field transition is, most probably, of the exchange origin. Using the results of a 1D frustrated model, we suggest that the observed high field transition from a spiral magnetic phase is the transition to a collinear spin-modulated magnetic phase.

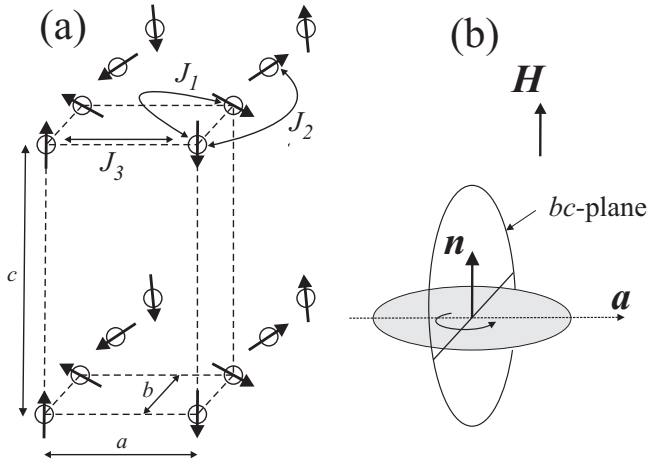

FIG. 1: (a) Schematic representation of the arrangement of Cu^{2+} moments in $LiCu_2O_2$. Only one of four Cu^{2+} (α, β, γ, δ) positions is shown. Arrows correspond to the spin directions below T_{c2}. J_1, J_2 and J_3 are the main exchange integrals[19]. (b) Scheme of the orientation of the spin plane for $\boldsymbol{H}$ in the (bc)–plane. $H > H_{c1}$. Spin plane is shadowed with gray. The direction of spin rotation by displacement along the chain (b–axes) is shown by the circular arrow. $\boldsymbol{n}$ is the vector normal to the spin plane.

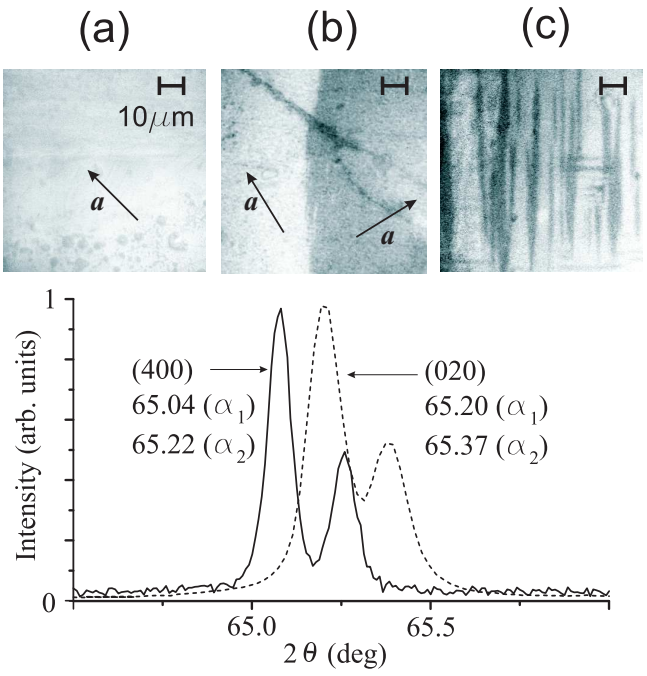

FIG. 2: Upper panel:Polarized optical microscope images of the (ab)–plane of $LiCu_2O_2$ samples (a) without twinning, (b) with two large twinned domains and (c) with complicated twinning structure. Lower panel: X-ray diffraction pattern observed in $\theta - 2\theta$ geometry on untwinned single crystal. The spectra were obtained from the (bc) and the (ac)–planes of the crystal.

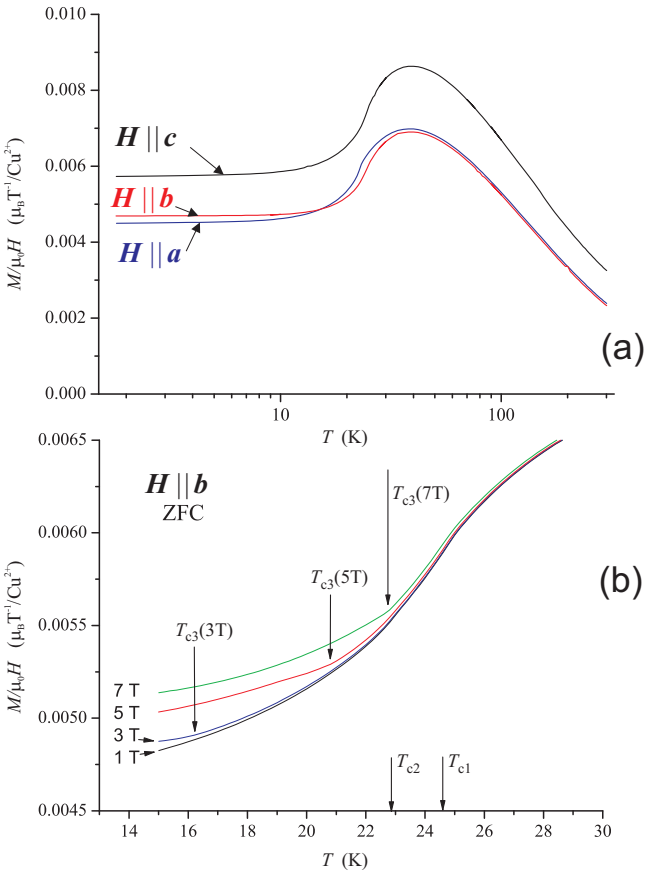

FIG. 3: (color online) Upper panel: Temperature dependence of the low field magnetization curves $M(T)/\mu_0 H$ for three field directions $\boldsymbol{H} \parallel \boldsymbol{a}, \boldsymbol{b}, \boldsymbol{c}$ and $\mu_0 H = 0.1$ T. Lower panel: $M(T)/\mu_0 H$ in the vicinity of the transition temperatures T_{c1} and T_{c2} at $\mu_0 H$ =1, 3, 5, and 7 T for $\boldsymbol{H} \parallel \boldsymbol{b}$.

II. CRYSTALLOGRAPHIC AND MAGNETIC STRUCTURES OF $LiCu_2O_2$

$LiCu_2O_2$ crystallizes in the orthorhombic lattice (space group $Pnma$) with the unit cell parameters a =5.73 Å, b =2.86 Å and c =12.42 Å.[21] The unit cell parameter a is approximately twice the unit cell parameter b. Consequently, the $LiCu_2O_2$ samples, as a rule, are characterized by the twinning due to formation of the crystallographic domains rotated by 90° around their common crystallographic axis c.

The unit cell of the $LiCu_2O_2$ crystal contains four univalent nonmagnetic cations Cu^+ and four divalent cations Cu^{2+} with the spin S=1/2. There are four equivalent crystallographic positions of the magnetic Cu^{2+} ions in the crystal unit cell of $LiCu_2O_2$, conventionally denoted as α, β, γ, and δ. The chains formed by one of four kinds of Cu^{2+} ions and relevant exchange interactions[19] within the system are shown schematically in Fig. 1(a).

The two-stage transition into a magnetically ordered state occurs at $T_{c1} = 24.6$ K and $T_{c2} = 23.2$ K.[23] Neutron scattering and NMR experiments have revealed an incommensurate magnetic structure in the magnetically ordered state ($T < T_{c1}$)[22,24,25]. The wave vector of the incommensurate magnetic structure coincides with the chain direction (b-axis). The magnitude of the propagation vector at $T < 17$ K is almost temperature independent and is equal to $0.827 \times 2\pi/b$. The neutron scattering experiments have shown that the magnetic moments neighboring along the a–direction are antiparallel, whereas those neighboring along the c–direction are coaligned. The intra-chain and inter-chain exchange constants were determined from the analysis of the spin wave spectra.[19] The nearest neighbour exchange interaction is ferromagnetic $J_1 = -7.00$ meV, while the next nearest neighbour exchange interaction is antiferromagnetic $J_2 = 3.75$ meV. The competition between these interactions leads to incommensurate magnetic structure. The antiparallel orientation of the magnetic moments of Cu^{2+} of the neighbouring chains is caused by the strong antiferromagnetic exchange interaction $J_3 = 3.4$ meV. The coupling of the Cu^{2+} moments along the c-direction and the couplings between the magnetic ions in different crystallographic positions are much weaker[19,24]. Thus, $LiCu_2O_2$ can be considered as a quasi-two dimensional. The quasi-two-dimensional character of magnetic interactions in $LiCu_2O_2$ compound was also proved by the resonant soft X-ray magnetic scattering experiments [26,27].

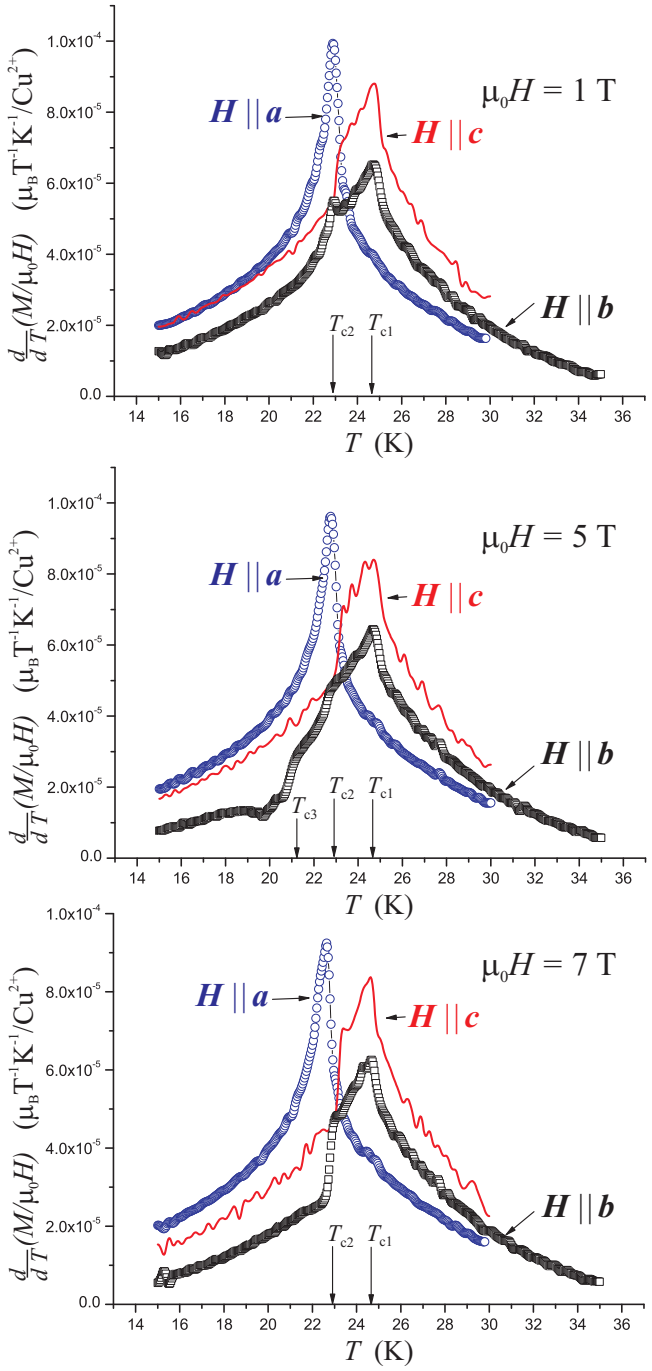

FIG. 4: (color online) Temperature dependences of the magnetization derivative dM/dT for three field directions in the vicinity of T_{c1} and T_{c2} obtained from $M(T)$ data at $\mu_0 H$ =1, 5, and 7 T.

Magnetic structure of $LiCu_2O_2$ at zero magnetic field was studied by several groups by means of neutron diffraction experiments[22,23,25]. The authors of Ref. 22 have proposed the planar spiral spin structure with the spins confined to the (ab)–plane. Polarized neutron scattering measurements of Ref.23 have detected the spin component along the c–direction, indicating the spiral magnetic structure in the (bc)–plane. The authors of Ref. 25, alternatively, have proposed a spiral spin structure confined to the (1,1,0) plane. It was attempted to extract information about magnetic structure of $LiCu_2O_2$ from the studies of electric polarization, which accompanies the magnetic ordering[23,28]. Unfortunately, at the moment, the nature of this polarization is not clear[29], which did not permit to obtain the definitive information about the zero-field magnetic structure from this type of experiment.

The magnetic structure realized in $LiCu_2O_2$ is much clearer in the magnetic fields above 3 T applied along $\boldsymbol{b}$ and $\boldsymbol{c}$ directions. ESR and NMR studies of $LiCu_2O_2$ in the low-temperature magnetically ordered phase ($T < T_{c2}$) have shown that the planar spiral magnetic structure is formed in this compound[20]. The magnetic moments located at the α (β, γ or δ) position of the crystal unit cell with coordinates x, y, z (measured along the a, b and c– axes of the crystal respectively) are defined as:

$$\boldsymbol{\mu}_\alpha = \mu \cdot \boldsymbol{l}_1(-1)^{x/a} \cdot \cos(k_{ic} \cdot y + \phi_\alpha) + \\ + \mu \cdot \boldsymbol{l}_2(-1)^{x/a} \cdot \sin(k_{ic} \cdot y + \phi_\alpha), \qquad (1)$$

where $\boldsymbol{l}_1$ and $\boldsymbol{l}_2$ are the two mutually perpendicular unit vectors, $\boldsymbol{k}_{ic}$ is the incommensurability vector parallel to the chain direction (b-axis) and μ is the magnetic moment of the Cu^{2+} ion. The ordered magnetic moment per copper ion at $T \lesssim 10$ K was evaluated as $\mu = 0.85\ \mu_B$.[20,22] The phases ϕ_α, ϕ_β, ϕ_γ and ϕ_δ determine the mutual orientation of the spins in the chains formed by the ions in the different crystallographic positions. Their values can be extracted from the NMR data[20,30].

III. SAMPLE PREPARATION AND EXPERIMENTAL DETAILS

Single crystals of $LiCu_2O_2$ with the size of several cubic millimeters were prepared by the solution in the melt method as described in Ref. 20. The samples had a shape of a flat plate with the developed (ab)–plane. The twinning structure of the samples was studied by the optical polarization microscopy. Typical views of the (ab)–plane of the samples are shown in Fig. 2. The dark and bright areas on the photos correspond to the domains with two different directions of the a–axis. In most cases, the samples were twinned with characteristic domain size of several microns (see Fig. 2(c)). It was possible to select the samples with large domains (see Fig. 2(b)) and the best samples were without twinning structure (Fig. 2(a)).

The absence of twinning structure in the samples selected for the experiments was confirmed by X-ray diffraction measurement(see lower panel of Fig. 2). The X-ray diffraction patterns were taken in $\theta - 2\theta$ geometry with use of CuK(α) irradiation. The untwinned crystal produced clearly distinguishable diffraction patterns from the (bc) and the (ac)–planes of the crystal (see lower

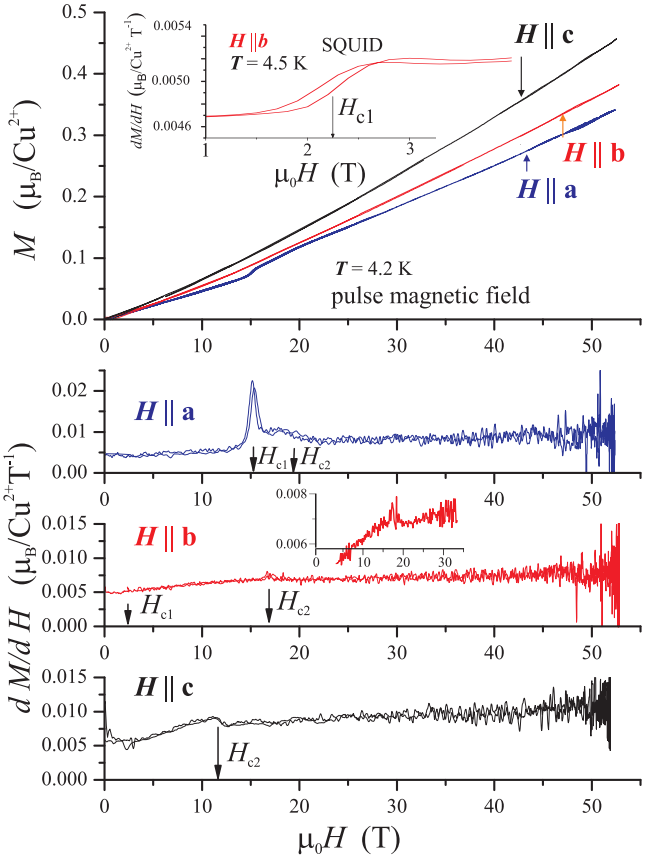

FIG. 5: (color online) Upper panel: Magnetization curves $M(H)$ at 4.2 K for three field directions $\boldsymbol{H} \parallel \boldsymbol{a}, \boldsymbol{b}, \boldsymbol{c}$ measured in pulse magnetic fields of up to 52 T. The inset shows the field dependence of dM/dH at 4.5 K for $\boldsymbol{H} \parallel \boldsymbol{b}$ measured with a SQUID magnetometer. Lower panels: Measured magnetic field dependences of dM/dH for the principal field directions $\boldsymbol{H} \parallel \boldsymbol{a}, \boldsymbol{b}, \boldsymbol{c}$. The inset shows the enlarged dependency in the range of transition field H_{c2} for $\boldsymbol{H} \parallel \boldsymbol{b}$.

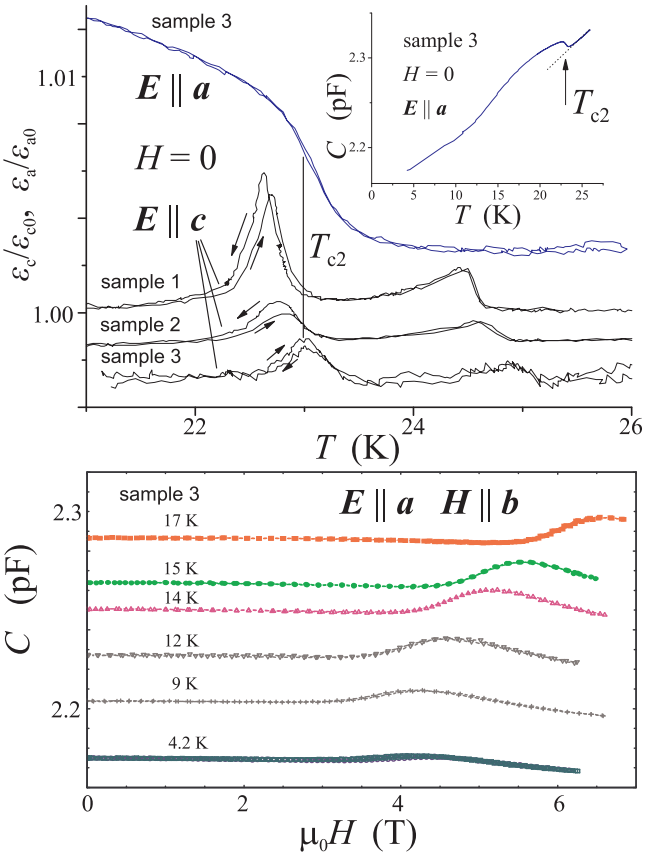

FIG. 6: (color online) Upper panel: Temperature dependences of dynamic dielectric constants of three samples at zero magnetic field for alternating electric field $\boldsymbol{E} \parallel \boldsymbol{a}, \boldsymbol{c}$. Dependences $\varepsilon(T)$ presented in the main panel were obtained by subtraction of the linear temperature drifts. Curves are shifted along the y-direction for better presentation. Insert shows the raw temperature dependence of the capacitance $C(T)$ for $\boldsymbol{E} \parallel \boldsymbol{a}$ at $H = 0$ with the linear extrapolation of $C(T)$ at $T > T_c$ to the range of $T \lesssim T_{c2}$ shown by dotted line. Lower panel: The field dependences of the capacitance for $\boldsymbol{E} \parallel \boldsymbol{a}$ and the magnetic field $\boldsymbol{H} \parallel \boldsymbol{b}$ at different temperatures. The data in the lower panel are plotted without shift along the y-axis.

panel of Fig. 2). The spectra obtained from twinned samples had a form of superposition of these spectra. ESR measurements also confirm absence of twinning in the samples used[20].

Magnetization curves in static magnetic fields of up to 7 T were measured with a commercial SQUID magnetometer (Quantum Design MPMS-XL7). High field magnetization data were taken in magnetic fields of up to 52 T using a pulsed magnet at KYOKUGEN in Osaka University.[31]

The dielectric constant ε was obtained from the four-contact capacitance measurements at 10 kHz on the capacitor formed by contact plates attached to the sample. The naturally grown samples with the flat (ab)–planes were used for the measurements of ε_c. Samples for the measurements of ε_a and ε_b were properly cut from the single crystals without twinning structure. Capacitor plates were formed right on the sample surface either by the sputtering of the silver film, or with the silver paste.

Different samples from the same batch were used for the dielectric constant and magnetization measurements, these samples are further denoted as "sample 1-5".

IV. EXPERIMENTAL RESULTS

A. Magnetization measurements at low fields

The experimental curves $M(T)/\mu_0 H$ and their temperature derivatives for three field directions $\boldsymbol{H} \parallel \boldsymbol{a}, \boldsymbol{b}, \boldsymbol{c}$ at $\mu_0 H = 0.1$ T are shown in Figs. 3 and 4. For all three field directions, there is a broad maximum of $M(T)/\mu_0 H$ at $T = 38$ K which is a typical feature of low-dimensional antiferromagnets. In the paramagnetic region, magnetic susceptibility for $\boldsymbol{H} \parallel \boldsymbol{c}$ exceeds that

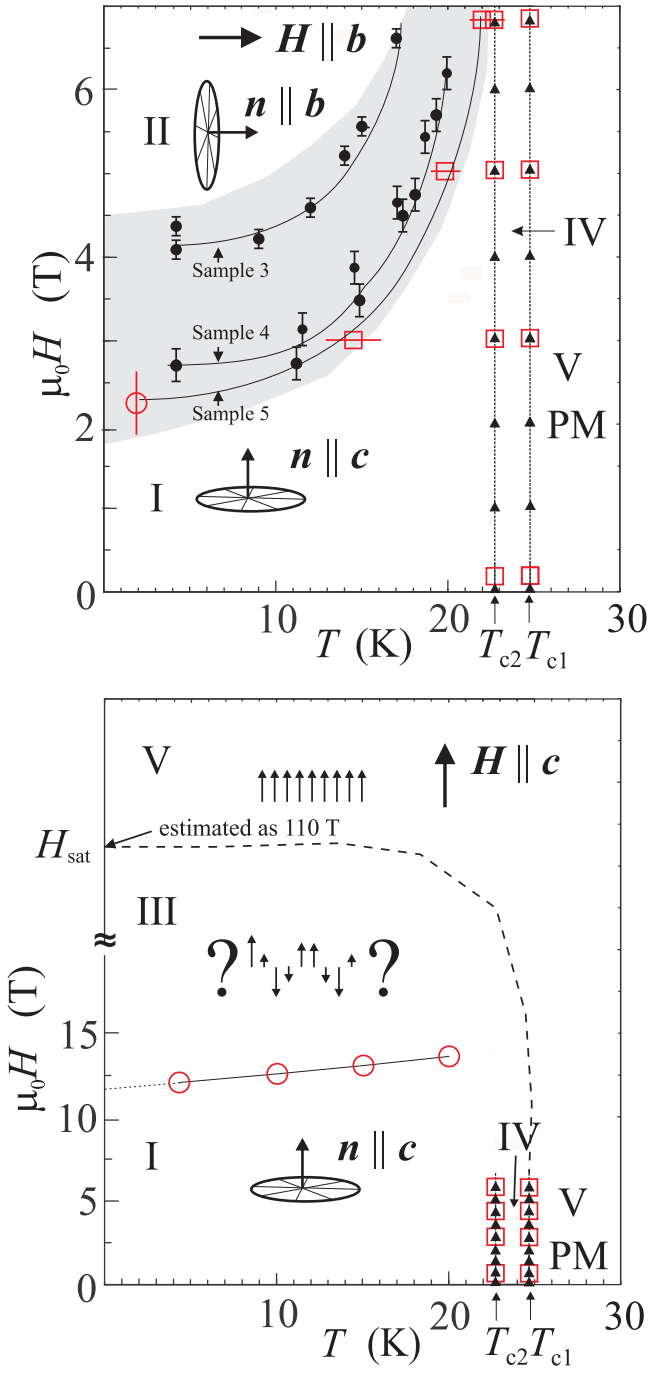

FIG. 7: (color online) Magnetic phase diagrams of $LiCu_2O_2$ compound for $\boldsymbol{H} \parallel \boldsymbol{b}$ (upper panel) and $\boldsymbol{H} \parallel \boldsymbol{c}$ (lower panel). The different symbols in the figures correspond to the data from different experimental methods. Solid triangles and circles show the phase boundaries obtained from $\varepsilon_c(T)$ and $\varepsilon_a(H)$ measurements, respectively. Open red circles and squares show the phase boundaries obtained from $M(H)$ and $M(T)$ measurements, respectively. The solid lines are guides to the eye. The grey shadowed area in the upper panel marks sample-dependent position of the phase boundary between phases I and II. High field spin structure III schematically shown in the phase diagram is merely speculative. Dashed line is a schematic phase boundary between the paramagnetic polarized and the ordered phases.

for $\boldsymbol{H} \parallel \boldsymbol{a}, \boldsymbol{b}$, which is consistent with the anisotropy of the g-tensor measured in ESR experiments[32] ($g_{a,b} = 2.0$; $g_c = 2.2$). The magnetic susceptibilities are temperature independent for $T \ll T_N$. The absence of significant paramagnetic contribution at low temperatures indicates low concentration of the uncontrolled magnetic impurities.

The transitions to the magnetically ordered states at T_{c1} and T_{c2} are marked by the change of the $M(T)$ slope. These inflection points are well resolved on the temperature derivative of $M/\mu_0 H$ (Fig. 4). The $\frac{d}{dT}(M/\mu_0 H)$ curves are strongly anisotropic. For $\boldsymbol{H} \parallel \boldsymbol{b}$ and $\boldsymbol{c}$, there are two anomalies corresponding to two transitions at T_{c1} and T_{c2}. The temperature dependence of $\frac{d}{dT}(M/\mu_0 H)$ for $\boldsymbol{H} \parallel \boldsymbol{a}$ shows only one sharp peak at the temperature near T_{c2} in all studied field range. An additional anomaly was observed on the $M(T)$ curves for $\boldsymbol{H} \parallel \boldsymbol{b}$ and $\mu_0 H \gtrsim 3$ T (lower panel of Fig. 3). At the transition temperature T_{c3}, the slope of $M(T)$ changes abruptly. The value of T_{c3} increases with the increase of magnetic field and merges with T_{c1} at $H \gtrsim 6$ T.

B. High-field magnetization measurements

The upper panel of Fig. 5 demonstrates magnetization $M(H)$ curves measured in pulsed fields of up to 52 T for $\boldsymbol{H} \parallel \boldsymbol{a}, \boldsymbol{b}, \boldsymbol{c}$. These curves were obtained by integrating the dM/dH curves presented in the lower three panels of Fig. 5.

The dM/dH curves show two anomalies which are marked as H_{c1} and H_{c2}. The anomaly at H_{c1} was observed for $\boldsymbol{H} \parallel \boldsymbol{a}$ and for $\boldsymbol{H} \parallel \boldsymbol{b}$. It is characterized by the increase of the $dM(H)/dH$, which may indicate a spin-reorientation transition. At the second transition field H_{c2}, observed in all three principal orientations, the field derivative of magnetization decreases.

The position of the critical field H_{c1} for the $\boldsymbol{H} \parallel \boldsymbol{b}$ corresponds to the magnetic transition at the temperature T_{c3} observed in the temperature scan of magnetization. The transition field H_{c1} is strongly anisotropic: for the $\boldsymbol{H} \parallel \boldsymbol{a}$, $\mu_0 H_{c1} = 15$ T, while for the $\boldsymbol{H} \parallel \boldsymbol{b}$ it varies from 2 to 5 T from sample to sample and demonstrates a hysteresis. The differential susceptibility dM/dH increases stepwise at the transition field H_{c1} by 65 ± 5 % for $\boldsymbol{H} \parallel \boldsymbol{a}$ and by 10 ± 3% for $\boldsymbol{H} \parallel \boldsymbol{b}$.

The second transition field H_{c2} is less anisotropic, its values are $\mu_0 H_{c2} = 15.3, 16.7$ and 11.5 T for the $\boldsymbol{H} \parallel \boldsymbol{a}, \boldsymbol{b}, \boldsymbol{c}$, respectively. At this transition the differential susceptibility decreases stepwise by 25 ± 3 %, 3 ± 1% and 11 ± 2% for the $\boldsymbol{H} \parallel \boldsymbol{a}, \boldsymbol{b}, \boldsymbol{c}$, respectively.

C. Dielectric constant measurements

Magnetic and electric properties of $LiCu_2O_2$ are strongly coupled[23,28]. The magnetic transitions are accompanied by anomalies of the dielectric constant.

The temperature and field dependences of the dielectric constant measured in our experiments are shown in Fig. 6. These curves were obtained from the temperature dependences of the capacitance. Linear drift obtained by extrapolation of $C(T)$ at $T > T_c$ was subtracted for better presentation. The example of the raw $C(T)$ curve and its high temperature linear extrapolation is given on the insert to Fig. 6. The temperature drift depends on the quality of capacitor plates contact with the sample. The strongest temperature drifts were observed for samples prepared for measurements at $E \parallel \boldsymbol{a}, \boldsymbol{b}$. In these cases the samples were composed from 10 or more oriented parts fastened with glue.

There are clearly visible anomalies on $\varepsilon(T)$ at $E \parallel \boldsymbol{a}, \boldsymbol{c}$ while there is no anomaly at $E \parallel \boldsymbol{b}$. The $\varepsilon_c(T)$ demonstrates two peaks at T_{c1} and T_{c2} as shown in the upper panel of Fig. 6. These peaks correspond to the two successive transitions between the paramagnetic phase and the ordered spiral one. The anomaly at T_{c1} has no hysteresis, while the $\varepsilon_c(T)$ shows hysteresis near T_{c2}. The positions of the peaks of $\varepsilon_c(T)$ varies from the sample to the sample in the range of 24.7 ± 0.2 K and 22.7 ± 0.2 K for T_{c1} and T_{c2}, respectively. The peak value of the dielectric constant changes by the factor of 10 depending on the sample. The $\varepsilon_a(T)$ shows only one broad, steplike anomaly around T_{c2}. The positions of the peak of $\varepsilon_c(T)$ and of the maximal slope of $\varepsilon_a(T)$ coincide for the same sample. No anomalies on the temperature and field dependences of ε_b were observed.

One broad peak is observed in the field dependence of capacitance C of $LiCu_2O_2$ sample for $\boldsymbol{H} \parallel \boldsymbol{b}$ and $\boldsymbol{E} \parallel \boldsymbol{a}$ (lower panel of Fig. 6), which corresponds to the transition at T_{c3} and H_{c1} on the corresponding $M(T)$ and $M(H)$ dependences (see Figs. 3 and 5).

D. Phase diagram

The $H-T$ magnetic phase diagram of $LiCu_2O_2$ is presented in Fig. 7. In total, it contains 5 different phases: (I) the low-field phase, (II) the phase above H_{c1} for $\boldsymbol{H} \parallel \boldsymbol{b}$, (III) the phase above H_{c2} for $\boldsymbol{H} \parallel \boldsymbol{c}$, (IV) the intermediate ordered phase between T_{c1} and T_{c2}, (V) the polarized paramagnetic phase.

The anomalies in $M(H)$, $M(T)$, $\varepsilon_a(T)$, $\varepsilon_a(H)$ which indicate the transition from the phase I to the phase II on the phase diagram have a hysteretic character. The phase boundaries obtained for three different samples for $\boldsymbol{H} \parallel \boldsymbol{b}$ are also shown on the phase diagram. The boundary between phases I and II for $\boldsymbol{H} \parallel \boldsymbol{b}$ changes with the sample.

V. DISCUSSION

To define the orientation of the spin plane in the space, it is convenient to introduce the vector normal to the spin plane $\boldsymbol{n} = [\boldsymbol{l}_1 \times \boldsymbol{l}_2]$, where $\boldsymbol{l}_1$ and $\boldsymbol{l}_2$ are the order parameter components introduced in Eq.(1). Orientation of the spin plane in a magnetic field is determined by the competition of the anisotropy of magnetic susceptibility and the crystal anisotropy. The Zeeman energy and energy of magnetic anisotropy for planar spiral spin structure can be written as:

$$E = -\frac{\chi_\perp}{2}H^2 - \frac{\chi_\parallel - \chi_\perp}{2}(\boldsymbol{n}\cdot\boldsymbol{H})^2 + a_1 n_x^2 + a_2 n_y^2, \quad (2)$$

where $\chi_\parallel$, $\chi_\perp$ are magnetic susceptibilities for field applied parallel and perpendicular to vector $\boldsymbol{n}$ (or, perpendicular and parallel to the spin plane, correspondingly). The constants of anisotropy are positive and $a_1 > a_2 > 0$; x and y axes are aligned along the a and b axes, correspondingly. Such choice of parameters ensures at zero field planar spiral structure with $\boldsymbol{n} \parallel \boldsymbol{c}$, as it was suggested in Ref.22.

As it was argued above, the phase transition at H_{c1} from the phase I to the phase II is the reorientation transition. The observation of spin reorientations for two field directions $\boldsymbol{H} \parallel \boldsymbol{a}$, $\boldsymbol{H} \parallel \boldsymbol{b}$ is possible only for $\chi_\parallel > \chi_\perp$: the spiral structure rotates in strong field to provide $\boldsymbol{n} \parallel \boldsymbol{H}$. The critical fields for the $\boldsymbol{H} \parallel \boldsymbol{a}, \boldsymbol{b}$ can be obtained by minimizing of the energy (Eq. 2) over the direction of the vector

$$\boldsymbol{H} \parallel \boldsymbol{a}: \quad H_{c1} = \sqrt{\frac{2a_1}{\chi_\parallel - \chi_\perp}}, \quad (3)$$

$$\boldsymbol{H} \parallel \boldsymbol{b}: \quad H_{c1} = \sqrt{\frac{2a_2}{\chi_\parallel - \chi_\perp}}, \quad (4)$$

The values of $\mu_0 H_{c1}$ for $\boldsymbol{H} \parallel \boldsymbol{a}$ and $\boldsymbol{H} \parallel \boldsymbol{b}$ differ essentially: 15 T and $\approx 1.8 - 4.2$ T respectively (see phase diagram on Fig. 7). Thus, we can conclude that $a_1/a_2 \approx 12 - 70$. The anisotropy parameters a_1 and a_2 define also the frequencies of electron spin resonance (ESR). The spin reorientation transition at $\mu_0 H_{c1} \approx 16$ T for $\boldsymbol{H} \parallel \boldsymbol{a}$ was predicted from the ESR data[20]. Our high field M(H) experiments provide direct experimental proofs for this predicted transition at $\mu_0 H_{c1} \approx 15$ T.

The two stage transition from the paramagnetic phase to the planar spiral phase is specific for the magnetic systems with a strong "easy plane" magnetic anisotropy for the vector $\boldsymbol{n}$.[34] This scenario is applicable to the case of $LiCu_2O_2$ since $a_1 \gg a_2$. Thus, $LiCu_2O_2$ can be approximately considered as a magnetic system with uniaxial anisotropy. For these systems at $T_{c2} < T < T_{c1}$, only one component of the order parameter of the spiral structure appears ($\mathbf{l_1} \parallel \mathbf{a}$, see Eq.(1)) and the other is fluctuating, while both components order at $T < T_{c2}$.

Peculiarity of the crystal a-direction is also confirmed by the magnetization measurements. The temperature

derivatives of the magnetization (Fig.4) for $\boldsymbol{H} \parallel \boldsymbol{b}, \boldsymbol{c}$ are similar to each other, and they demonstrate sharp anomalies both at T_{c1} and at T_{c2}. In the same time, the dM/dT curve for $\boldsymbol{H} \parallel \boldsymbol{a}$ changes essentially only at T_{c2}.

In the high field range, the second phase transition was observed at H_{c2}. This transition is accompanied by the decrease of the susceptibility and is observed for all three principal field directions. This fact suggests the exchange origin of this transition. At H_{c2}, a spiral structure in individual chains probably changes to the other one. Such a transition from the spiral to collinear spin-modulated phase was observed recently in the quasi-one dimensional magnet with the same type of frustration $LiCuVO_4$.[33] For the quasi-one dimensional systems, this unusual magnetic phase was interpreted theoretically as a spin-density wave phase[7–9].

For the one dimensional frustrated chain with the exchange constants J_1 and J_2 of $LiCu_2O_2$ ($J_1/J_2 \approx -2$) corresponding transition is expected, according to Ref.7, at $H_{c2} \approx 0.2H_{sat}$. The value of H_{sat} is not known experimentally, but it can be evaluated by extrapolating the $M(H)$ dependences to the magnetization value equal to $gS\mu_B$ per Cu^{2+} ion. The linear extrapolation of $M(H)$ gives the upper estimate for the saturation field $H_{sat} \approx$130 T. Taking into account the 15 percents spin reduction in low field range, we can expect, that the saturation field will be $\approx 15\%$ less than the value derived from linear extrapolation: $H_{sat} \approx 110$ T. This results in the evaluation of the H_{c2} value of $\approx 20 - 25$ T which is close to the values observed in experiment. The theoretical consideration of the same 1D model in Ref. 8 predicts a transition to the spin-density wave phase at the value of magnetic moment $0.12M_{sat}$, which is also in the reasonable agreement with the experimentally observed value $\approx 0.07M_{sat}$ (see Fig. 5).

It is unclear how sensitive is the spin-density wave phase, predicted theoretically for 1D system, to the interchain exchange interaction J_3, which is essential for $LiCu_2O_2$. The effect of the interchain exchange interaction may be responsible for the difference between the results of the model calculations and experimental values of H_{c2}. Thus spin-density wave phase can be a plausible candidate for magnetic phase realized in $LiCu_2O_2$ at $H > H_{c2}$. More definite conclusion requires further experimental study of this phase.

Finally, it should be noted that the uniaxial anisotropy observed in $LiCu_2O_2$ is unclear at the moment and still awaits theoretical consideration.

VI. CONCLUSIONS

The low field magnetic phase transition observed on the untwinned $LiCu_2O_2$ crystals for the field aligned in the (ab)–plane of the crystal can be described as a reorientation transition of the spiral structure. The observed phase transitions are in agreement with the presence of the strong easy (bc)–plane anisotropy for vector $\boldsymbol{n}$ of spiral structure in $LiCu_2O_2$[20]. The origin of such strong anisotropy in $LiCu_2O_2$ at the moment is unknown. New high field magnetic transition was observed for the field directed along all three principal axes of the crystal. The critical field of this magnetic transition is close to the value of transition field from a spiral to a spin density wave structure predicted theoretically for one dimensional model with parameters of exchange interactions J_1 and J_2 expected for $LiCu_2O_2$.

Acknowledgments

This work was carried out under the Visiting Researcher Program of KYOKUGEN and partly supported by Grants-in-Aid for Scientific Research (No.20340089), the Global COE Program (Core Research and Engineering of Advanced Materials-Interdisciplinary Education Center for Materials Science) (No. G10) from the MEXT, Japan, by the Grants 12-02-00557-, 10-02-01105-a of the Russian Foundation for Basic Research, and Program of Russian Scientific Schools.

* Electronic address: svistov@kapitza.ras.ru

[1] A. V. Chubukov, Phys. Rev. B **44**, 4693 (1991).
[2] A. K. Kolezhuk, Phys. Rev. B **62**, R6057, (2000).
[3] A. K. Kolezhuk and T. Vekua, Phys. Rev. B **72**, 094424 (2005).
[4] T. Vekua, A. Honecker, H.-J. Mikeska, and F. Heidrich-Meisner, Phys. Rev. B **76**, 174420, (2007).
[5] D. V. Dmitriev and V. Yu. Krivnov, Phys. Rev. B **77**, 024401 (2008).
[6] F. Heidrich-Meisner, A. Honecker and T. Vekua, Phys. Rev. B **74**, 020403(R), (2006).
[7] T. Hikihara, L. Kecke, T. Momoi and A. Furusaki Phys. Rev. B **78**, 144404 (2008).
[8] J. Sudan, A. Lüscher, and A. M. Läuchli, Phys. Rev. B **80**, 140402(R) (2009).
[9] F. Heidrich–Meisner, I. P. McCulloch, and A. K. Kolezhuk, Phys. Rev. B **80**, 144417 (2009).
[10] S. Furukawa, M. Sato, Y. Saiga, and S. Onoda, J. Phys. Soc. Jpn. **77**,123712 (2008).
[11] S. Furukawa, M. Sato and S. Onoda, Phys. Rev. Lett. **105**, 257205, (2010).
[12] M. E. Zhitomirsky and H. Tsunetsugu, Europhys. Lett. **92**, 37001 (2010).
[13] S. Nishimoto, S. -L. Drechsler, R. Kuzian and J. van den Brink cond-mat, arXiv:1005.5500 (2010)
[14] M. Sato, S. Furukawa,S. Onoda and A. Furusaki, Mod. Phys. Lett. B **25**,901, (2011).
[15] M. Enderle, C. Mukherjee, B. Fäk, R. K. Kremer, J. -

M. Broto, H. Rosner, S. -L. Drechsler, J. Richter, J. Malek, A. Prokofiev, W. Assmus, S. Pujol, J. -L. Raggazzoni, H. Rakoto, M. Rheinstädter, H. M. Rønnow, Europhys. Lett. **70**, 237 (2005).

[16] M. Hase, H. Kuroe, K. Ozawa, O. Suzuki, H. Kitazawa, G. Kido, and T. Sekine, Phys. Rev. B **70** 104426 (2004).

[17] S. -L. Drechsler, O. Volkova, A. N. Vasiliev, N. Tristan, J. Richter, M. Schmitt, H. Rosner, J. Málek, R. Klingeler, A. A. Zvyagin, and B. Büchner, Phys. Rev. Lett. **98** 077202 (2007).

[18] M. G. Banks, F. Heidrich-Meisner, A. Honnecker, H. Rakoto, J. -M. Broto, R. K. Kremer, J. Phys.: Condens. Matter **19**, 145227 (2007).

[19] T. Masuda, A. Zheludev, B. Roessli, A. Bush, M. Markina, and A. Vasiliev, Phys. Rev. **72**, 014405 (2005).

[20] L. E. Svistov, L. A. Prozorova, A. M. Farutin, A. A. Gippius, K. S. Okhotnikov, A. A. Bush, K. E. Kamentsev, and É. A. Tishchenko, JETP **108**, 1000 (2009).

[21] R. Berger, A. Meetsma, S. v. Smaalen, J. Less-Common Met. **175**, 119, (1991).

[22] T. Masuda, A. Zheludev, A. Bush, M. Markina, and A. Vasiliev, Phys. Rev. Lett. **92**, 177201 (2004).

[23] S. Seki, Y. Yamasaki, M. Soda, M. Matsuura, K. Hirota, and Y. Tokura, Phys. Rev. Lett. **100**, 127201 (2008).

[24] A. A. Gippius, E. N. Morozova, A. S. Moskvin, A. V. Zalessky, A. A. Bush, M. Baenitz, H. Rosner, and S. -L. Drechsler, Phys. Rev. **70**, 020406 (2004).

[25] Y. Kobayashi, K. Sato, Y. Yasui, T. Moyoshi, M. Sato, and K. Kakurai, J. Phys. Soc. Jpn. **78**, 084721 (2009).

[26] A. Rusydi, I. Mahns, S. Müller, M. Rübhausen, S. Park, Y. J. Choi, C. L. Zhang, S. -W. Cheong, S. Smadici, P. Abbamonte, M. v. Zimmermann, and G. A. Sawatzky, Appl. Phys. Lett. **92**, 262506 (2008).

[27] S. W. Huanga, D. J. Huanga, J. Okamoto, W. B. Wu, C. T. Chen, K. W. Yeh, C. L. Chen, M. K. Wu, H. C. Hsu, F. C. Chou,, Sol. State Com. **147**, 234 (2008).

[28] S. Park, Y. J. Choi, C. L. Zhang, and S. -W. Cheong, Phys. Rev. Lett. **98** 057601 (2007).

[29] A. S. Moskvin, Yu. D. Panov, and S. -L. Drechsler, Phys. Rev. B **79**, 104112 (2009).

[30] L. E. Svistov, L. A. Prozorova, A. A. Bush, K. E. Kamentsev, J. Phys.: Conf. Series **200**, 022062 (2010).

[31] M. Hagiwara, S. Kimura, H. Yashiro, S. Yoshii and K. Kindo, J. Phys. Conf. Ser. **51**, 647 (2006).

[32] A. M. Vorotynov, A. I. Pankrats, G. A. Petrakovskii, K. A. Sablina W. Paszkowicz and H. Szymczak, JETP **86**, 1020 (1998).

[33] N. Büttgen, H. -A. Krug von Nidda, L. E. Svistov, L. A. Prozorova, A. Prokofiev, W. Assmus, Phys. Rev. B **76**, 014440 (2007).

[34] M. Mochizuki and N. Furukawa, Phys. Rev. Lett. **105**, 187601 (2010).